

MONOLITHIC INTEGRATION OF RELEASED AND SOLIDLY MOUNTED RF ACOUSTIC DEVICES ON HETEROGENEOUS SUBSTRATE

Jinbo Wu^{1,2,3,#}, Shibin Zhang^{1,#,*}, Hongyan Zhou^{1,2}, Liping Zhang^{1,2}, Pengcheng Zheng^{1,2}, Hulin Yao^{1,2}, Xiaomeng Zhao¹, Kai Huang¹, Tao Wu^{3,*}, Xin Ou^{1,2,*}

¹The State Key Laboratory of Functional Materials for Informatics, Shanghai Institute of Microsystem and Information Technology, Shanghai 200050, CHINA

²The Center of Materials Science and Optoelectronics Engineering, University of Chinese Academy of Sciences, Beijing 100049, CHINA and

³ShanghaiTech University, Shanghai 201210, CHINA

ABSTRACT

This work first presents the monolithic integration of the solidly mounted surface acoustic wave (SAW) devices and the released Lamb wave devices on the Y128-cut LiNbO₃-on-silicon (LNOSi) substrate. The Rayleigh mode SAW resonators showing a phase velocity (v_p) of about 3700 m/s and effective electromechanical coupling coefficients (k_{eff}^2) between 7.3% to 9.5% are suitable for low-frequency and small-band filters, while the first order antisymmetric Lamb wave (A1) resonators showing scalable v_p from 9476 m/s to 15280 m/s and k_{eff}^2 between 9.2% to 23.4% are suitable for mid-, high-frequency and large-bandwidth filters. The A1 mode and Rayleigh mode filters were also fabricated and measured, exhibiting 3-dB fractional bandwidths (FBW) of 5.5% and 2.4% around 2.1 GHz, respectively. The hybrid acoustic devices with complementary properties on LNOSi substrate show a great potential for applications in the hundred-filter sub-6 GHz RF front-ends.

KEYWORDS

Acoustic filter, Monolithic integration, LiNbO₃-on-silicon (LNOSi), Hybrid acoustic device.

INTRODUCTION

Acoustic device is one of the most important components of 5G radio frequency (RF) front-ends [1]-[7]. With the development of wireless communication technology, the number of filters in the RF front-end modules of high-end smartphones has grown to 50 to 100. At this stage, die-level surface acoustic wave (SAW) and bulk acoustic wave (BAW) filters with different structures (on various piezoelectric substrates), designs, and incompatible manufacturing processes are usually integrated using highly customized flip-chip processes, which are costly, complicated, and large-sized. In order to maintain the current size of smartphones, denser RF front-end modules with a smaller footprint are required.

Surface acoustic wave (SAW) resonators are widely applied in wireless communications due to the low cost and simple manufacturing process [1], [6], [8]-[11]. Most importantly, the operating frequency of SAW devices is defined by lithography, which promotes the integration of SAW devices enabling multiband operations on a single substrate. However, their operating frequency is limited by the phase velocity (v_p) of the target mode (e.g., Rayleigh mode, shear horizontal mode) while their bandwidth is limited by the effective electromechanical coupling

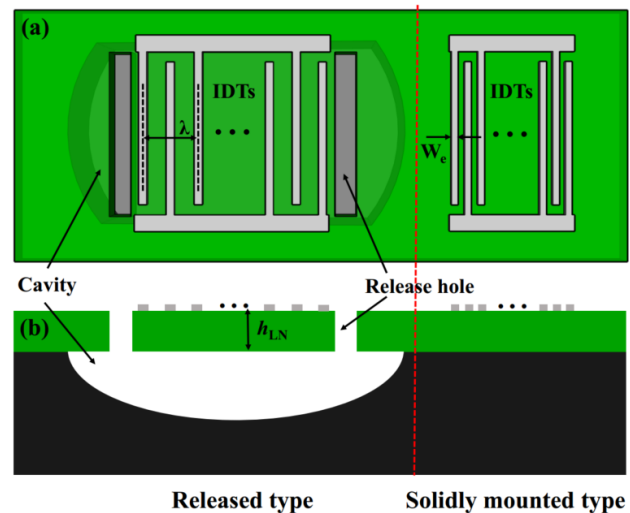


Figure 1. (a) Top and (b) cross-sectional views of the schematic of monolithically integrated hybrid acoustic devices.

coefficients (k_{eff}^2). The thin film bulk acoustic wave resonators (FBAR) can be applied to higher frequency bands due to the extremely high phase velocities of the bulk waves [5]-[12]. Since the frequency of a BAW device is inversely proportional to the thickness of the sandwiched piezoelectric layer (e.g., AlN, AlScN), BAW devices for multiple bands require the precisely controlled piezoelectric layers of various thicknesses as well as the complicated fabrication processes. Acoustic devices based on piezoelectric heterogeneous substrates have achieved breakthrough performances in recent years. Lamb wave resonators (LWRs) based on released piezoelectric films have recently received widespread attention because of the higher v_p , larger k_{eff}^2 and lithography-defined frequency. To high frequency bands, LWRs have the advantages of small size, large bandwidth, and multiple frequency bands available on a single substrate [13]-[17]. Then to low frequency bands, LWRs require a large suspended active area to increase the capacitance to match the 50 Ω terminal, which will result in a more fragile structure and a larger form factor. When acoustic devices with different structures can be monolithically integrated on a single substrate (as shown in Figs. 1(a) and (b)), the filter modules covering low, medium and high frequency bands will be realized.

In this work, the Rayleigh mode SAW resonators (solidly mounted) and the first order antisymmetric Lamb

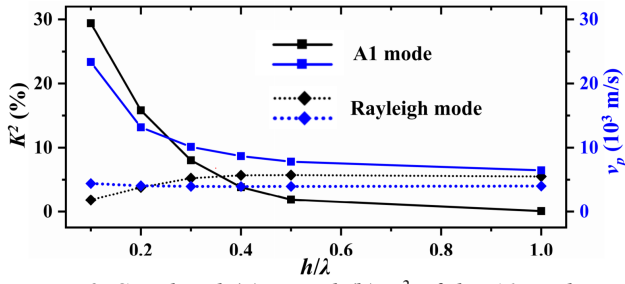


Figure 2. Simulated (a) v_p and (b) K^2 of the A1 mode and Rayleigh mode resonators with different h/λ .

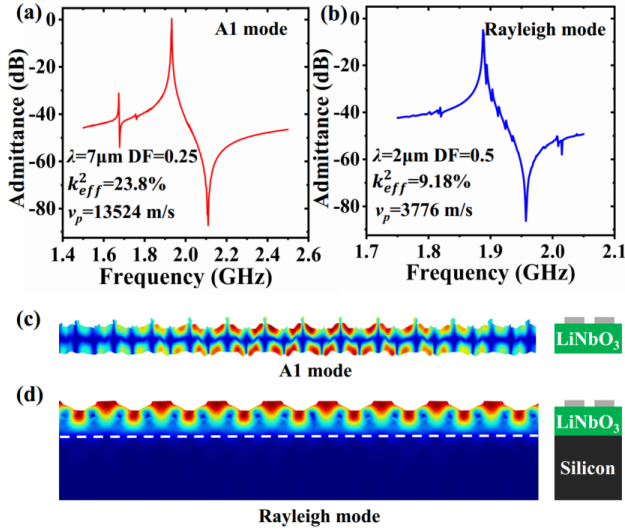


Figure 3. Simulated admittance curves of the (a) A1 mode and (b) Rayleigh mode resonators. Displacement mode shapes of the (c) A1 mode and (d) Rayleigh mode resonators.

wave resonators (A1 LWRs, released) with complementary v_p and k_{eff}^2 were monolithically integrated on the Y128-cut LiNbO₃-on-silicon (LNOSi) substrate. In addition, acoustic filters of solidly mounted and released were also successfully demonstrated within the compatible process flow, showing great potentials in filters of multiple frequency bands in 5G front-ends.

DEVICE DESIGN AND SIMULATION

The structures of the A1 LWR and Rayleigh SAW resonator are shown in Figs. 1(a) and (b). Both structures contain interdigital transducers (IDTs), but only LWRs have release holes and cavities. The coexistence of released and solidly mounted resonators can be achieved by selectively etching through the release holes. To obtain a maximum k_{eff}^2 , Y128-cut LiNbO₃ was selected as the piezoelectric material and the x-axis was selected as the propagation orientation of the A1 mode and Rayleigh mode.

To analyze the dispersion characteristics of the A1 mode and Rayleigh mode, resonators based on LNOSi substrate with different ratio of the thickness of LiNbO₃ (h_{LN}) to wavelength (λ) were simulated by 3-D finite element analysis (FEA). The phase velocity v_p and intrinsic electromechanical coupling (K^2 , directly related to k_{eff}^2 [18]) calculated by eigenmode analysis are shown in Fig. 2. K^2 is defined by $(v_m^2 - v_0^2)/v_0^2$, where v_m and v_0 are the

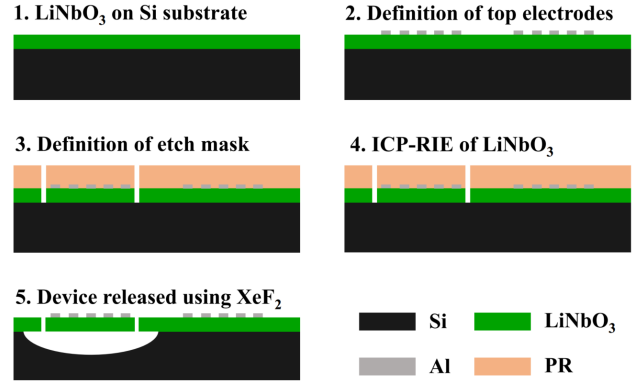


Figure 4: Fabrication process for the monolithically integrated hybrid acoustic devices.

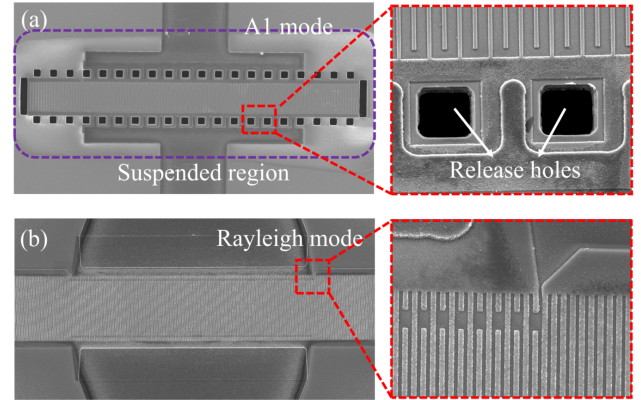


Figure 5: SEM images of the (a) A1 mode and (b) Rayleigh mode resonators.

phase velocities of the target mode in LiNbO₃ plates with metallized and free surface boundary conditions, respectively. Rayleigh mode usually requires a larger ratio of film thickness to wavelength (h/λ) to obtain a larger k_{eff}^2 , while the A1 mode is opposite. When h/λ is small, the v_p of A1 mode will be several times higher than that of Rayleigh mode. By setting the proper h/λ and performing selectively releasing of the piezoelectric thin film, it is possible to excite different acoustic modes with diverse v_p and k_{eff}^2 on a single heterogeneous substrate. This means that the filters on a single substrate can achieve wider frequency coverage under the same lithography resolution. The typical simulated admittance curves and the corresponding displacement mode shapes of two modes are shown in Fig 3, proving the complementarity in v_p and k_{eff}^2 .

FABRICATION AND MEASUREMENT

The monolithic integration of the released A1 mode and the solidly mounted Rayleigh SAW devices were achieved within the process flow shown in Fig. 4. First, the Y128-cut LiNbO₃ thin film was transferred onto a silicon substrate. Then the aluminum electrodes were defined on top of the LiNbO₃ film through electron beam lithography, metal evaporation and lift-off process. Next, the photoresist SPR220-7 was patterned on the surface of LiNbO₃ film as a hard mask. Then the LiNbO₃ thin film was subsequently etched through by ICP-RIE to form the release windows of the A1 mode devices. Finally, the silicon underneath the LiNbO₃ was removed by XeF₂-based dry etching to achieve

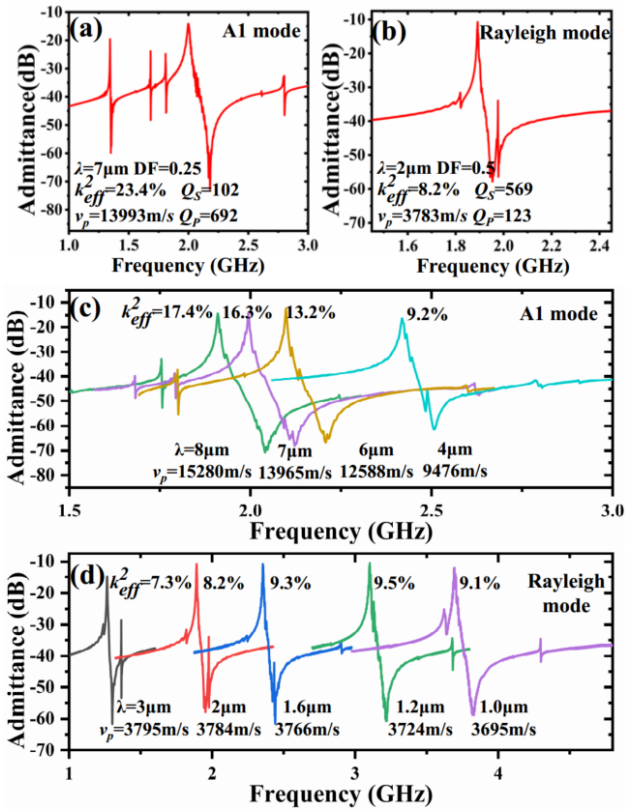


Figure 6. The measured admittance curves of the typical (a) A1 mode and (b) Rayleigh mode resonators. Measured admittance curves of the (c) A1 mode and (d) Rayleigh mode resonators with different λ .

the suspension of A1 mode devices. At the same time, the Rayleigh mode devices still maintain a solidly mounted state. The SEM images of the A1 mode and Rayleigh mode resonators are shown in Figs. 5(a) and (b), respectively, in which a relatively thick LiNbO₃ film ($h_{\text{LN}}=1.2\ \mu\text{m}$) was used to get a large k_{eff}^2 of the Rayleigh mode and 150 nm aluminum electrodes were used here for lower ohmic loss.

The frequency responses of the fabricated acoustic devices were characterized using a vector network analyzer (Keysight E5071C) with a terminal impedance of 50 Ω at room temperature in air. The measured admittance curves of the typical Rayleigh mode and A1 mode resonators are shown in Figs. 6(a) and (b), in which the above modes exhibit v_p of 3783 m/s and 13993 m/s, respectively. The large velocity difference between the two modes makes it possible to achieve wider frequency coverage on a single substrate. The measured admittance curves and the extracted k_{eff}^2 and v_p of the fabricated A1 mode and Rayleigh mode resonators with different λ are shown in Figs. 6(c) and (d), respectively, where the electrode linewidth (W_e) of the A1 mode resonators is maintained at 0.5 μm , while the duty factor ($\text{DF}=2W_e/\lambda$) of the Rayleigh SAW is 0.5. The A1 mode resonators exhibit scalable resonances from 1.91 to 2.42 GHz, and the corresponding k_{eff}^2 between 9.2% and 17.4%. As the wavelength decreases (i.e., h/λ increases), the k_{eff}^2 and v_p of the A1 mode decrease significantly (dispersion), which is consistent with the simulation results. In that case, thinner LiNbO₃ film should be used to increase the frequency of A1 mode without

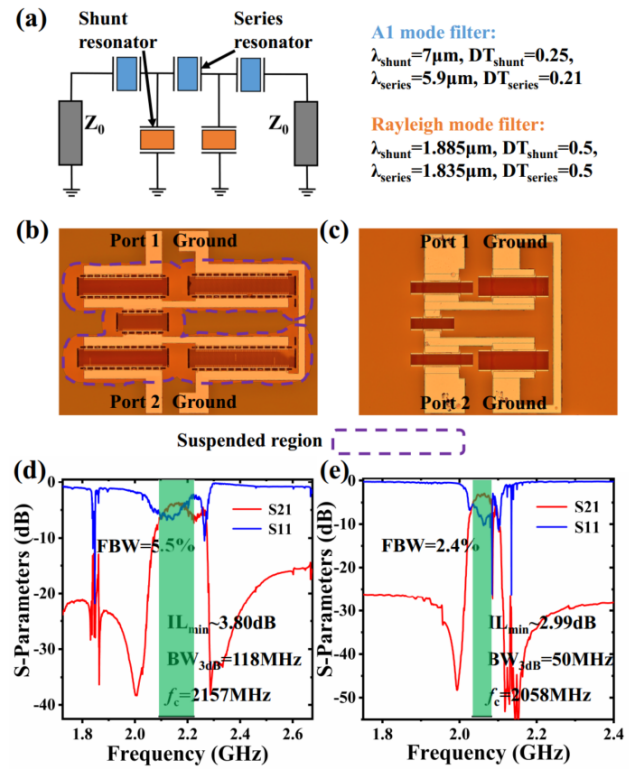


Figure 7. (a) The topology of a ladder filter ($Z_0=50\Omega$). OM images of the (b) A1 mode and (c) Rayleigh mode filters. S-Parameters of the (d) A1 mode and (e) Rayleigh mode filters.

decreased k_{eff}^2 . The Rayleigh mode resonators exhibit scalable resonances from 1.27 to 3.70 GHz, and the corresponding k_{eff}^2 between 7.3% and 9.1%. When the wavelength is less than 3 μm (h/λ is larger than 0.4), the Rayleigh mode has a moderate k_{eff}^2 and almost constant v_p , which can meet the requirements of most frequency bands at low and medium frequencies.

Based on the measured results of above resonators, the A1 mode and Rayleigh mode filters were also designed and fabricated. Fig. 7(a) shows the topology of the filters. The shunt (series) resonators with a wavelength of 7 (5.9) μm was chosen to build the A1 mode ladder-type filter. At the same time, the wavelengths of the shunt and series resonators of the Rayleigh mode filter are 1.885 μm and 1.835 μm , respectively. The optical microscope (OM) images and the measured S-parameters of the filters are shown in Figs. 6(b)~(e), respectively. The A1 mode filter features a center frequency (f_c) of 2.157 GHz, a 3-dB fractional bandwidth (FBW) of 5.5% and a minimum insertion loss (IL_{min}) of 3.8 dB. The Rayleigh mode filter features a f_c of 2.058 GHz, a FBW of 2.4% and an IL_{min} of 2.99 dB. The A1 mode filter exhibits large insertion loss and in-band ripples due to the non-uniformity of the thickness of LiNbO₃ thin film. After further optimizations in device design and fabricated process, it can be expected to realize the high performance monolithic multi-filter module on LNOSi substrate for RF front-ends.

CONCLUSION

In this work, the solidly mounted surface acoustic

wave (SAW) devices and released lamb wave devices were monolithically integrated on Y128-cut LNOSi substrate. The measured resonators of A1 mode and Rayleigh mode exhibit scalable resonances from 1.27 to 3.70 GHz, and the corresponding k_{eff}^2 between 7.3% and 17.4%. Filters of two modes were also fabricated and measured, exhibiting 3-dB fractional bandwidths (FBW) of 5.5% and 2.4% around 2.1 GHz, respectively. After further optimization, the hybrid acoustic devices with complementary properties on LNOSi substrate will be promising for monolithic multi-frequency applications in RF wireless communications.

ACKNOWLEDGEMENTS

This work was supported by the National Key R&D Program of China (2020YFB2008802, 2019YFB1803901, 2019YFB1803902, 2019YFB1803903), National Natural Science Foundation of China (61874128, 61851406, 11705262, 61874073), Frontier Science Key Program of CAS (QYZDY-SSW-JSC032, ZDBS-LY-JSC009), Chinese–Austrian Cooperative R&D Project (GJHZ201950), Program of Shanghai Academic Research Leader (19XD1404600), K. C. Wong Education Foundation (GJTD-2019-11).

REFERENCES

- [1] E. Butaud, T. Laroche, V. Barec, A. Clairet, and C. Didier, "A Single Smart Cut POI Substrate Design for UHF, L and S Band Filters," in 2020 50th European Microwave Conference (EuMC), 2021.
- [2] S. Gong and G. Piazza, "Monolithic Multi-Frequency Wideband RF Filters Using Two-Port Laterally Vibrating Lithium Niobate MEMS Resonators," *Journal of Microelectromechanical Systems*, vol. 23, no. 5, pp. 1188-1197, 2015.
- [3] K. Y. Hashimoto, M. Kadota, T. Nakao, M. Ueda, and K. Suzuki, "Recent Development of Temperature Compensated SAW Devices," in *Ultrasonics Symposium (IUS)*, 2011 IEEE International, 2011.
- [4] M. Kadota and S. Tanaka, "Ultra-wideband ladder filter using SH0 plate wave in thin LiNbO3 plate and its application to tunable filter," *IEEE Transactions on Ultrasonics Ferroelectrics & Frequency Control*, vol. 62, no. 5, p. 939, 2015.
- [5] Y. Shen, P. Patel, R. Vetry, and J. B. Shealy, "452 MHz Bandwidth, High Rejection 5.6 GHz UNII XBAW Coexistence Filters Using Doped AlN-on-Silicon," in 2019 IEEE International Electron Devices Meeting (IEDM), 2019.
- [6] Y. Takamine, T. Takai, H. Iwamoto, T. Nakao, and M. Koshino, "A Novel 3.5 GHz Low-Loss Bandpass Filter Using I.H.P. SAW Resonators," in 2018 Asia-Pacific Microwave Conference (APMC), 2018.
- [7] S. Zhang, R. Lu, H. Zhou, S. Link, and S. Gong, "Surface Acoustic Wave Resonators Using Lithium Niobate on Silicon Carbide Platform," in 2020 IEEE/MTT-S International Microwave Symposium (IMS), 2020.
- [8] T. H. Hsu, K. J. Tseng, and M. H. Li, "Large Coupling Acoustic Wave Resonators Based on LiNbO3/SiO2/Si Functional Substrate," *IEEE Electron Device Letters*, vol. PP, no. 99, pp. 1-1, 2020.
- [9] J. Shen, S. Fu, R. Su, H. Xu, and F. Pan, "High-Performance Surface Acoustic Wave Devices Using LiNbO/SiO/SiC Multilayered Substrates," *IEEE Transactions on Microwave Theory and Techniques*, vol. PP, no. 99, pp. 1-1, 2021.
- [10] V. Yantchev, P. J. Turner, S. Mchugh, F. Iliev, and C. H. Lee, "Parametric study of resonant TC-SAW piston-mode configurations," in 2017 IEEE International Ultrasonics Symposium (IUS), 2017.
- [11] H. Zhou, S. Zhang, Z. Li, K. Huang, and X. Ou, "Surface Wave and Lamb Wave Acoustic Devices on Heterogenous Substrate for 5G Front-Ends," in 2020 IEEE International Electron Devices Meeting (IEDM), 2020.
- [12] M. Hodge, R. Vetry, S. R. Gibb, M. Winters, and J. B. Shealy, "High rejection UNII 5.2GHz wideband bulk acoustic wave filters using undoped single crystal AlN-on-SiC resonators," in 2017 IEEE International Electron Devices Meeting (IEDM), 2017.
- [13] H. Campanella, Y. Qian, C. O. Romero, J. S. Wong, and R. Kumar, "Monolithic Multiband MEMS RF Front-End Module for 5G Mobile," *Journal of Microelectromechanical Systems*, vol. PP, no. 99, pp. 1-9, 2020.
- [14] G. Chen, C. Cassella, W. Tao, and M. Rinaldi, "Single-chip multi-frequency wideband filters based on aluminum nitride Cross-sectional Lamé mode resonators with thick and apodized electrodes," in *The 31st IEEE International Conference on Micro Electro Mechanical Systems, MEMS 2018*, 2018.
- [15] Gong, Songbin, Piazza, and Gianluca, "Figure-of-Merit Enhancement for Laterally Vibrating Lithium Niobate MEMS Resonators," *IEEE Transactions on Electron Devices*, 2013.
- [16] R. Lu, Y. Yang, S. Link, and S. Gong, "A1 Resonators in 128° Y-cut Lithium Niobate with Electromechanical Coupling of 46.4%," *Journal of Microelectromechanical Systems*, vol. PP, no. 99, pp. 1-7, 2020.
- [17] P. Turner, B. Garcia, V. Yantchev, G. Dyer, and V. Plessky, "5GHz Band n79 wideband microacoustic filter using thin Lithium Niobate membrane," *Electronics Letters*, 2019.
- [18] S. Gong and G. Piazza, "Design and Analysis of Lithium–Niobate-Based High Electromechanical Coupling RF-MEMS Resonators for Wideband Filtering," *IEEE Transactions on Microwave Theory & Techniques*, vol. 61, no. 1, pp. 403-414, 2013.

CONTACT

- *Shibin Zhang, sbzhang@mail.sim.ac.cn
- *Tao Wu, wutao@shanghaitech.edu.cn
- *Xin Ou, ouxin@mail.sim.ac.cn
- *Corresponding authors
- #Authors contributed equally to this work